# The effect of dense gas dynamics on loss in ORC transonic turbines



2017 J. Phys.: Conf. Ser. 821 012021

(http://iopscience.iop.org/1742-6596/821/1/012021)

IOP Conf. Series: Journal of Physics: Conf. Series **821** (2017) 012021 doi:10.1088/1742-6596/821/1/012021

# The effect of dense gas dynamics on loss in ORC transonic turbines

**FJ Durá Galiana[1], APS Wheeler[2], J Ong[3] and CA de M Ventura[2]**

[1]Aerodynamics and Flight Mechanics, Engineering and the Environment, University of Southampton, Southampton, SO17 1B, UK
[2]Whittle Laboratory, Department of Engineering, Cambridge University, Cambridge, UK
[3]GE Global Research, Munich, Germany

E-mail: fjdg1g08@soton.ac.uk

**Abstract.** This paper describes a number of recent investigations into the effect of dense gas dynamics on ORC transonic turbine performance. We describe a combination of experimental, analytical and computational studies which are used to determine how, in-particular, trailing-edge loss changes with choice of working fluid. A Ludwieg tube transient wind-tunnel is used to simulate a supersonic base flow which mimics an ORC turbine vane trailing-edge flow. Experimental measurements of wake profiles and trailing-edge base pressure with different working fluids are used to validate high-order CFD simulations. In order to capture the correct mixing in the base region, Large-Eddy Simulations (LES) are performed and verified against the experimental data by comparing the LES with different spatial and temporal resolutions. RANS and Detached-Eddy Simulation (DES) are also compared with experimental data. The effect of different modelling methods and working fluid on mixed-out loss is then determined. Current results point at LES predicting the closest agreement with experimental results, and dense gas effects are consistently predicted to increase loss.

## 1. Introduction

Organic Rankine Cycle (ORC) engines are widely used in power generation and heat recovery industrial processes. This is due to the good performance of ORC engines when producing power from low temperature heat sources. In order to increase the power density produced by the engine they commonly have a high pressure single stage turbine. Due to the configuration of the turbine, flows typically reach high Mach numbers at the trailing-edge of the vane resulting in large losses. Moreover the fluids used in ORC engines are typically Dense gases which present strong real gas and dense gas effects within the high pressure turbines.

The study of dense gas flow within the turbine is an emerging field of study. Only a few studies have looked at viscous effects in dense gas flows; these generally tend to show reduced viscous effects within the dense gas region [1, 2, 3, 4, 5]. However, it is unclear whether this is due to an increase of Reynolds number within the dense gas region. Generally, these studies do not consider trailing-edge loss which is a major input to turbine loss. In a single stage transonic turbine up to a third of the loss produced is originated downstream of the vane trailing-edge [6].

Recent investigations [7, 8] have shown that within the dense gas region the size of the base flow separation at the trailing-edge is significantly reduced as compared to gases outside this region. It was concluded that, while the viscous contribution to loss seemed to be significantly

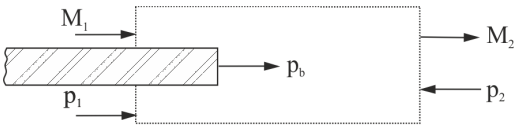


**Figure 1.** Control volume of a flat plate in a wind tunnel.

reduced within the dense gas region, the loss was dependent on the viscous-inviscid interaction, and this was largely dependent on the fundamental derivative ($\Gamma = 1 + \frac{\rho}{a}\left(\frac{\partial a}{\partial \rho}\right)_s$). This paper aims to determine how we can accurately model these flows and investigates the effect of trailing-edge shape on turbine vane performance. This investigation is divided into three parts. First, an analytical investigation of real gas effects on trailing-edge flows; secondly, an experimental validation of a computational simulation for dense gas trailing-edge flows; and, lastly, an investigation on the effects of trailing-edge shape on an ORC turbine vane.

## 2. 1D inviscid analysis of trailing edge flows

Denton & Xu [9] show that it is possible to predict the loss of a transonic trailing-edge in air using an inviscid Euler computation, as long as it predicts correctly the average suction surface pressure. In this section the authors extend this theory to Dense gas flows. In the Denton & Xu analysis of a transonic flow over a flat plate, they look at the control volume shown in Fig. 1. The Mach number upstream of the trailing edge is $M_1 = 1$, the inlet pressure is kept constant and the downstream pressure is varied to achieve a range of pressure ratios and downstream mixed-out states. Assuming an adiabatic choked flow, where the mass is conserved and viscous effects on the control volume boundaries are neglected it can be shown that for an ideal gas $P_{\circ 2}/P_{\circ 1} = (A_1 F(M_1))/(A_2 F(M_2))$, where $F(M)$ is the non-dimensional mass flow as a function of Mach number, and total temperature is conserved ($T_{\circ 1} = T_{\circ 2}$). However, these temperature and pressure relations are only valid for an ideal gas. For any real-gas where the equation of state is known, the same conservation laws can be used to determine the downstream stagnation pressure and temperature, if the downstream static pressure is specified. Using these results, the base pressure can be determined from the momentum balance as:

$$p_b t_{t.e.} = m(V_2 - V_1) + p_2 A_2 - p_1 A_1. \tag{1}$$

Using these same assumptions and conservation of mass, momentum and energy, and using real gas thermodynamic models, it is possible to determine the mixed-out loss ($\zeta = \frac{H_2 - H_{2S}}{H_{\circ 1} - H_{2S}}$) for the case of a dense-gas flow over a trailing-edge. Hence a 1-dimensional study on a transonic trailing-edge flow over a flat plate using these relations is presented; ideal gas relations were used for air, and thermodynamic properties for dense gases were produced using the National Institute of Standards and Technology (NIST) real gas routines (REFPROP) [10]. All predictions are for single phase gas flows. The selected trailing-edge blockage was chosen to match that of the experiments carried out here ($A_2/A_1 = 0.237$). All dense gas flows have been expanded from initial reduced conditions of $p/p_c = 0.3245$ and $T/T_c = 0.952$. For these calculations the trailing-edge total pressure, $p_{o,in}$, and temperature and the Mach number, $M_1$, are set and the static properties of the flow are obtained from these assuming isentropic expansion from stagnation conditions. Following this, a range of downstream mixed-out static pressures, $p_2$, is set and flow properties are calculated for the whole range using the relations previously described.

Figure 2 shows the relationship between loss coefficient and base pressure as the downstream Mach number ($M_2$) is increased from a subsonic to supersonic value. Moving along these lines from the subsonic branch ($M_2 < 1$) to the supersonic branch ($M_2 > 1$), as the downstream Mach number is increased, the base pressure drops and the loss rises up to a peak maximum. However, the peak loss does not occur where the base pressure is lowest; the minimum base pressure occurs when $M_2 = 1$, while the peak loss occurs in the region of $M_2 = M_{2\text{peak}} = 0.78 - 0.81$ and

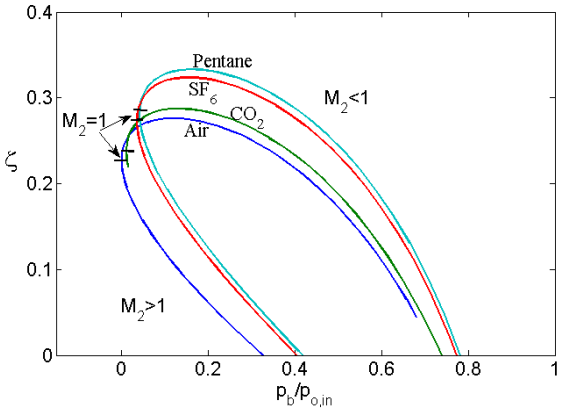


**Figure 2.** Loss coefficient variation with base pressure for air, $CO_2$, $SF_6$ and pentane with a trailing-edge Mach number of $M_1 = 1$.

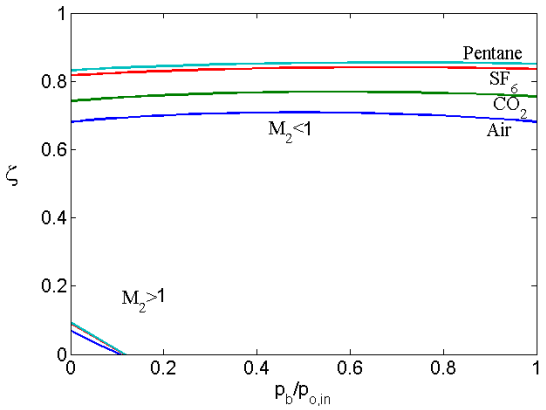


**Figure 3.** Loss coefficient variation with base pressure for air, $CO_2$, $SF_6$ and pentane with a trailing-edge Mach number of $M_1 = 2$.

$p_b = 0.12 - 0.16$. Thus, there is a small region between the maximum $M_2$ and $M_2 = 1$, where the loss reduces as base pressure drops. The results show that in general, dense gas effects tend to increase base pressure but at the same time raise trailing-edge loss for a given base pressure.

The same analysis was performed on flows for which the inlet Mach number is higher than unity. Figure 3 shows the variation in loss coefficient with base pressure for a case where the trailing-edge Mach number was $M_1 = 2$ for Air, $CO_2$, $SF_6$ and pentane. Here, there is a range of mixed-out conditions ($M_2$ and $p_2$) for which base pressure and loss coefficient achieve values which are not physically possible, and there is a discontinuity in the physical solutions on the loss-$p_b$ curve. This discontinuity separates the subsonic and supersonic branches of the curve. For both cases ($M_1 = 1$ and $M_1 = 2$), there is a significant range of base pressure for which two solutions of the loss coefficient could exist. As a result of this, loss coefficient cannot be determined based solely on the base pressure. It is also shown here that dependence of loss on base pressure is greatly reduced for the subsonic branch as compared for the first case where $M_1 = 1$. Generally, dense gas effects increase loss, except for a small region in the supersonic branch where $M_2 > 2.1$.

These results show that for solutions along the subsonic branch, the maximum loss when $M_1 = 1$ is typically 60% lower than the $M_1 = 2$ case. However, a 20% reductions in fundamental derivative will typically raise maximum loss by 20% both when $M_1 = 2$ and $M_1 = 1$. Hence, the sensitivity of trailing-edge loss to dense gas effects is weakly dependent on the choice of vane-exit Mach number for the range of chosen fundamental derivatives.

In order to determine the dependence of trailing-edge loss on dense gas behaviour further, a set of experiments and CFD studies are presented next.

## 3. Experimental set-up

The experimental results have been obtained using a Ludwieg tube facility capable of producing high speed flows at a range of temperatures [7, 8]. The Ludwieg tube has three main parts: a 7.5m charge tube (⌀50mm), a 0.4m test section and a 150 litre reservoir tank. In a Ludwieg tube configuration the diaphragm is placed between the test section and the reservoir tank downstream; consequently, the charge tube and test section are pressurized together. The diaphragms have been calibrated to burst at desired pressures.

$SF_6$ is the chosen dense gas for the study, as it has similar thermodynamic properties and behaviour to pentane, which is a widely used gas in ORC systems [7, 8]. For the experiments

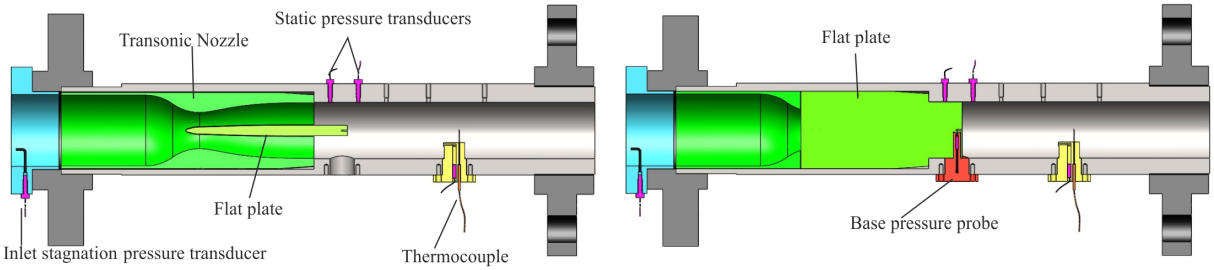


**Figure 4.** Test section and nozzle with embedded plate modified for base pressure measurements in free-stream static pressure (left) and base pressure (right) measurement configurations.

performed with $SF_6$ a "DILO B052R11 $SF_6$-gas" service cart was used to recover in full the used gas. All gases were tested at $M \approx 2.0$ and a Reynolds number based on the trailing-edge conditions and thickness of the flat-plate trailing-edge ($Re \approx 1 \times 10^6$) obtaining a range of fundamental derivative values; $\Gamma_{\text{Air}} = 1.2$, $\Gamma_{\text{CO2}} = 1.13\text{-}1.15$ and $\Gamma_{\text{SF6}} = 0.99\text{-}1.04$. $\Gamma$ values represent the range values of $\Gamma$ from the throat of the nozzle to the flat-plate trailing-edge at the specified conditions for each gas; these where determined using REFPROP for $CO_2$ and $SF_6$. Air is assumed to be an ideal gas.

The experiment designed for this study is a continuation of the work previously done on the study of trailing-edge wake flows [7, 8]. Similarly, a supersonic trailing-edge flow was produced by a flat plate embedded in a transonic nozzle which accelerates isentropically the flow up to an exit Mach number of 2 (see Fig. 4). The nozzle has been produced by an in-house code which accounts for the dense gas effects in supersonic flows and has been previously validated [7, 8]. The flat-plate was designed to include a base pressure measurement as shown in Fig. 4.

A "Kulite XCL-62" pressure transducer was used to capture the base pressure and "Kulite XTEL-140" transducers were used to measure wall static and inlet total pressures. All pressure transducers are fast-response transducers sampled at 100kHz using the National Instruments' "USB-6356 X-series DAQ" data acquisition system. All probes were calibrated and tested using the high precision modular pressure controller GE PACE5000. Due to the short run times ($t_{\text{run}} = 30\text{-}100$ms) temperature was difficult to measure accurately within the runs, so pre-run measurements were taken using a fast response needle type "OMEGA HYP0" probe.

## 4. Computational set-up

Three different computational studies were produced; the first study is a CFD simulation of the flat plate in the Ludwieg tube where the results where compared with the experimental results. The second computational study is an ORC vane flow. Lastly a trailing-edge shape study was conducted on the ORC vane geometry with the aim to determine how shape affects the base flow and loss. The software used for flow solving was FLUENT v14.5. Steady and unsteady simulations were performed using the density based solver. Simulations were performed using the third order MUSCL implicit algorithm and unsteady simulations were performed using a dual-time-stepping method. Air was computed assuming an ideal gas behaviour. The equations of state for Pentane, $CO_2$ and $SF_6$ were given by the NIST real gas data base within ANSYS.

RANS modelling was used for steady simulations using the vorticity based Spalart-Allmaras (SA) turbulence model; Other RANS models were also compared, but no significant differences in wake prediction were observed. LES were performed for the unsteady simulations. For this the Smagorinsky-Lilly model was employed, where $C_s = 0.1$ and $Pr_{wall} = 0.85$. A mesh and time-step dependency study is discussed later. DES simulations were also performed using the vorticity based SA RANS model; this is due to uncertainty of the impact of using wall functions in the described flows. Flat plate DES simulations were only performed using air.

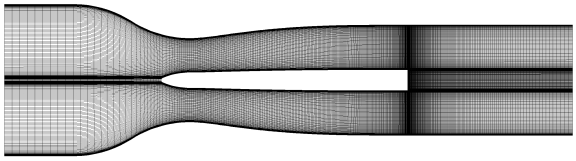

**Figure 5.** Nozzle with embedded plate mesh (symmetry plane).

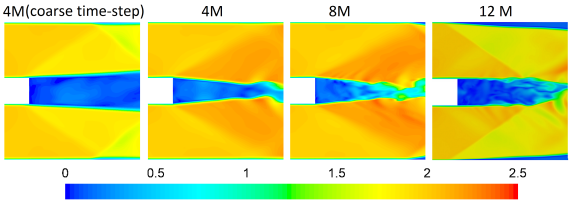


**Figure 6.** Instantaneous LES predicted change in flow in the base region with varying mesh size in an air flow.

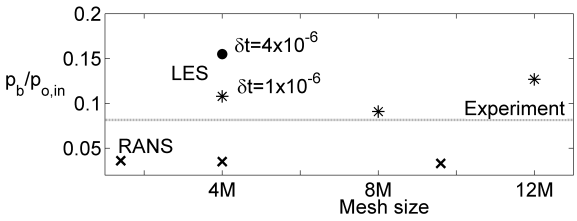


**Figure 7.** (above) Predicted base pressure for various RANS (×) and LES (•,∗) mesh and time-step sizes compared to measured base pressure for the air case.

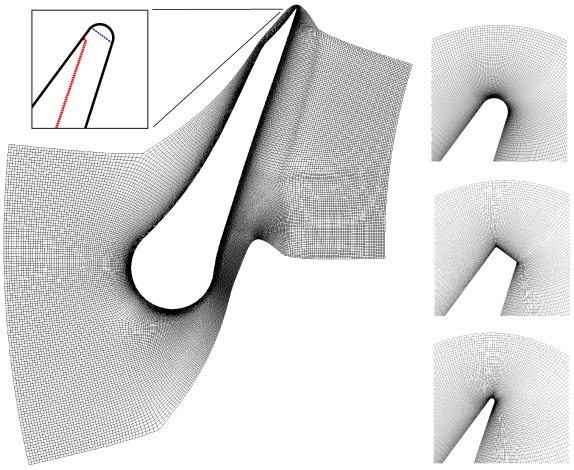

**Figure 8.** (right) ORC turbine vane baseline mesh and trailing-edge geometry variations.

The geometrical model for the flat plate study (see Fig. 5) is a representation of the geometry in the test section. Mesh sensitivity studies were carried out using RANS and LES with mesh sizes ranging from 0.7 to 12 million points. Over the plate surface, the near wall grid sizes were (on the region close to the trailing-edge for the air 8M mesh) $y^+ \approx 30$, $x^+ \approx 48$ and $z^+ \approx 88$. $y^+$ was selected to be consistent with the wall-function used within the solver. The use of wall functions was necessary due to the high Reynolds numbers and thus the prohibitively high computational cost of resolving the viscous sublayer. Furthermore, the focus of this work was the base region and not the surface flow.

Figure 6 shows how the trailing-edge flow changes with changes in time step size and mesh density. From left to right it can be seen that the size of the base region and wake width gets reduced as the time step size decreases and the mesh density increases. For the last case (12 million cells) it can be seen that the base region increases again to a rectangular shape. In this case, the boundary-layers on the outer walls of the domain appear to have increased significantly in thickness and the additional blockage is likely to be affecting the trailing-edge flow.

Figure 7 shows the experimentally measured and CFD predicted base pressure for air for different mesh and time-step sizes. It can be seen here that the accuracy of the base pressure is highly dependent on the selection of time-step size and mesh density for LES. The time-step size was initially defined to be 10 times smaller than the flow time-scale; this was estimated using the domain mass-averaged flow velocity and the domain length. The time-step size study determined that the optimum time-step size was $\delta t = 1\mu$s; this gave good agreement with the experiment results, while keeping computation costs to an acceptable level. An increase in mesh density improves the prediction initially, but it can cause a divergence from the experimental

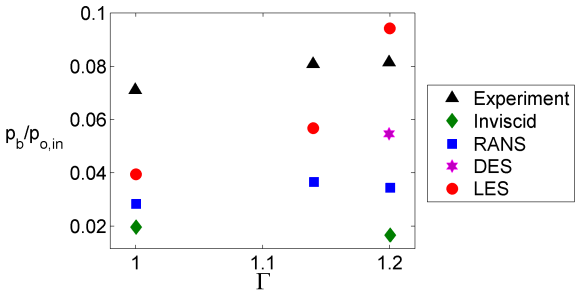


**Figure 9.** Base pressures for $SF_6$ ($\Gamma \approx 1$), $CO_2$ ($\Gamma \approx 1.14$) and air ($\Gamma \approx 1.2$).

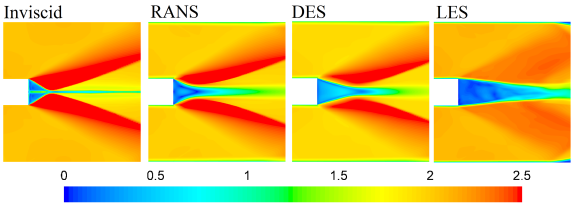


**Figure 10.** Predicted time-averaged Mach contours for air by inviscid, RANS, DES and LES CFD calculations.

results as seen for the 12 million cells mesh. This is likely to be due to the over-prediction of the outer wall boundary-layer blockage.

The final investigations involve the study of a typical turbine vane flow with pentane as the working fluid. The baseline geometry (Fig. 8) was designed in a previous ORC turbine study [6]. The vane was designed for a radial turbine operating with pentane with a mass flow rate of $2kg/s$, a temperature ratio of $T_{\circ,in}/T_{exit} = 1.15$, rotational speed of 26500RPM, power output of 155kW and a pressure ratio $p_{\circ,in}/p_{exit} = 11$ across the turbine. The inlet stagnation reduced conditions of the stage were $T_{\circ,in}/T_c = 0.96$ and $p_{\circ,in}/p_c = 0.59$, resulting in a range of fundamental derivative of $0.75 < \Gamma < 0.95$ across the vane.

For the current study the shape of the trailing-edge was modified to three different designs (Fig. 8) while the baseline model was kept unchanged. The three trailing edges used are: the original round trailing-edge, a square-cut trailing-edge, and a radial-cut trailing-edge. The latter is produced by a radial cut-away of the suction surface of the turbine vane. The square-cut trailing-edge is produced by cutting away the round trailing-edge producing a surface perpendicular to the pressure surface of the vane.

The meshing of the vane geometries (Fig. 8) was performed using similar mesh resolution for the flat-plate study as this is the mesh that has been validated to give acceptable results. Hence the wall $y^+$ along the surface of the vane has been set so that it is generally $y^+ \gtrsim 30$ and wall functions are used, and a similar mesh density has been produced at the trailing-edge, with 50 points along the trailing-edge height ($t_{\text{t.e.}} = 0.5\%c$) and 40 points along the span (span$= 5\%c$). The vane was produced using a Matlab script for the geometry and ANSYS turbogrid v14.5 for the meshing. The square and radial-cut trailing edges included a small corner radius of $r_{\text{corner}} = 0.04$mm. This is 14% of the round trailing edge thickness, $t_{\text{t.e.}}$.

## 5. Comparison of experiments and CFD results

Figure 9 shows base pressure CFD predictions and experimental measurements. Both the CFD and experimental data show that the base pressure reduces with decreasing fundamental derivative, this effect is specially seen between the $CO_2$ and the $SF_6$. Comparing the different CFD models it can be seen that, while the Inviscid and RANS modelling predictions give close results between them and agree with the trend seen in the experiments, the LES modelling gives a closer agreement with experiments. It can also be observed that DES for air predicts a base pressure in between RANS and LES.

Figure 10 shows contours of Mach number in the base region of the flat plate for the air case. Here it can be seen how as viscous modelling is introduced from Inviscid to RANS the size of the base region increases, as well as the wake width. Similarly, when scale-resolving methods are included with DES and LES the base region increases again. By comparing these plots to the values of base pressure given by each simulation, it can be seen that an increase in the size

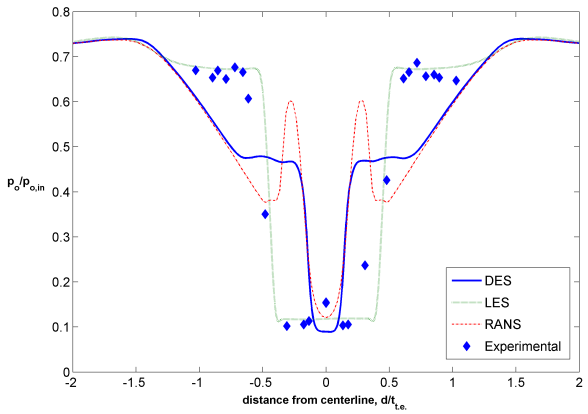


**Figure 11.** Measures and predicted shocked pressure profiles across the wake at a distance of $1.5t_{\text{t.e.}}$ downstream of flat-plate trailing-edge.

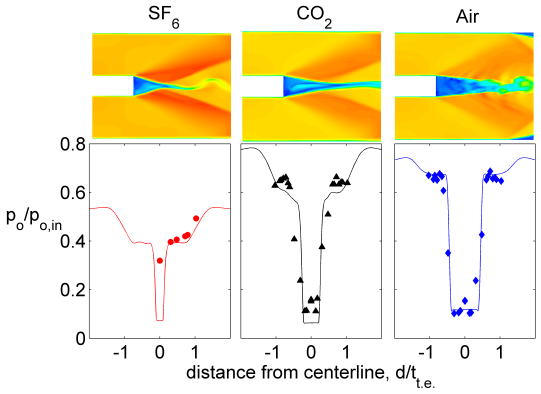


**Figure 12.** Measures and predicted shocked pressure profiles across the wake at a distance of $1.5t_{\text{t.e.}}$ downstream of flat-plate trailing-edge and contours of instantaneous Mach number at the trailing-edge.

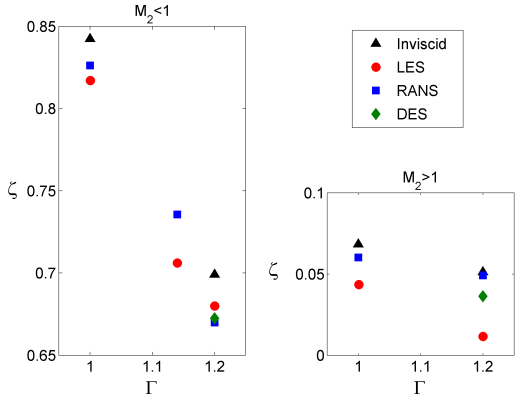


**Figure 13.** Predicted possible mixed-out loss coefficient for the three gases depending on the mixed out velocity $M_2$.

of the base region is accompanied by an increase in the base pressure.

Figure 11 shows a comparison of the measured experimental and CFD predicted wakes of air at a distance of $1.5t_{t.e.}$ downstream of the flat plate trailing-edge. The values of pressure in the profiles shown have been corrected to account for the total pressure drop across a normal shock and will be referred to as *shocked total pressures*. *Shocked total pressures* predicted by RANS, LES and DES modelling are shown. The figure shows that LES gives the closest agreement with the experimental measurements.

Figure 12 shows how a reduction in fundamental derivative produces a reduction in the size of the base region, which in-turn produces a reduction in base pressure as shown in Fig. 9. The smaller base region is produced as a result of an increasingly larger wake turning angle of the supersonic slipstream. This is directly related to the reduced Fundamental derivative in dense gases as shown in [7, 8]. Figure 12 also shows a comparison of the measured experimental and LES predicted wakes. As it can be seen here, the LES predictions in general matches the experimental measurements for all the studied flows. The results show a clear reduction in the wake size as the fundamental derivative decreases.

Figure 13 shows the possible predicted mixed-out loss coefficients for the three cases. These were calculated by using the momentum flux computed at the trailing-edge plane from the CFD calculations and the 1D analysis of a flat-plate flow discussed in the beginning of this paper. Following this mixed-out and base pressures were calculated for a range of downstream

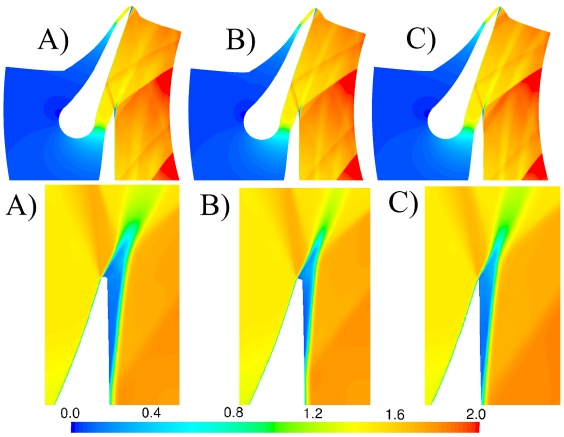


**Figure 14.** Predicted mean Mach numbers for pentane vane of various trailing-edge shapes: A) round, B) square-cut, C) radial-cut.

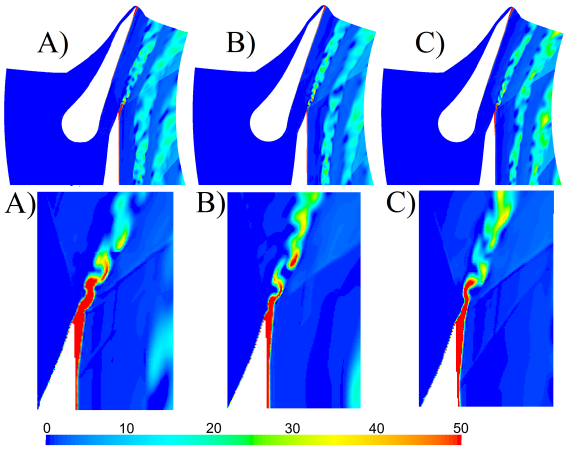


**Figure 15.** Predicted instantaneous entropy increase (J/kgK) for a pentane vane of various trailing-edge shapes: A) round, B) square-cut, C) radial-cut.

conditions. Finally, by using the CFD predicted base pressure, a set of possible mixed-out loss coefficients were calculated. As a result, two mixed-out loss coefficients are possible for the Air and $SF_6$, one of them belonging to the subsonic branch and the other one to the supersonic branch. On the other side, $CO_2$ only presented one possible solution of mixed-out loss coefficient with a subsonic mixed-out state.

The results show that the sensitivity of the predicted loss due to the viscous modelling is dependent on the final mixed-out Mach number; for subsonic solutions, the loss is much less dependent on viscous effects as compared to the supersonic solutions. In both cases, nonetheless, the trailing-edge loss is increased as the fundamental derivative is reduced.

## 6. The effect of trailing edge shape

The results obtained in the previous section are used here to provide an analysis of an ORC turbine vane. The emphasis of the study falls on the dependence of the flow features on the trailing-edge shape of a turbine vane.

Figure 14 shows a comparison of the time-averaged flowfields produced by the three different trailing-edge shapes. For all three cases the flow on the pressure side (P.S.) is expanded through the vane nozzle and around the trailing-edge ending up in a trailing-edge shock that impinges on the suction side (S.S.) of the adjacent vane. On the suction side of the vane there is a boundary-layer separation which occurs prior to the trailing-edge, and an oblique compression shock is generated. Further downstream, this merges with the compression shock formed at the confluence region of the base flow. The point of separation and strength of the subsequent oblique shock appears to be modified by the trailing-edge shape, and thus the size of the base region is dependent on the trailing-edge shape.

In the case of the square-cut trailing-edge, the point of separation occurs further downstream as compared to the other two cases (see Fig. 14). The base region produced by the square-cut geometry is also the smallest of the three cases. In the case of the radial-cut trailing-edge the point of separation occurs further upstream as compared to the other two cases, but the size of the base region is comparable to the separation produced by the round trailing-edge.

The major difference between the three cases is the over-expansion produced by the radial-cut trailing-edge. Since the radial cut modifies part of the suction surface as well as the trailing-

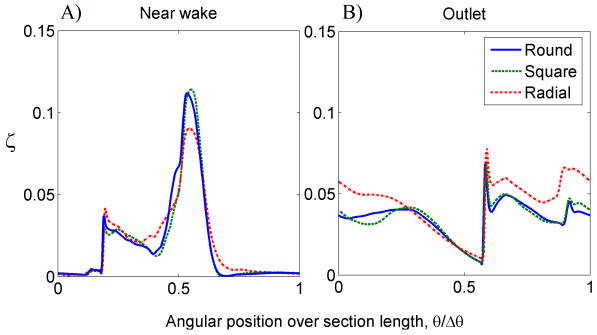


**Figure 16.** LES predicted time-averaged mass-weighted loss coefficient ($\zeta$) for a pentane vane of various trailing-edge shapes at $0.25c_r$ (A) and $1c_r$ (B) radial distances downstream of trailing-edge. $c_r$ is the radial length of the vane and $\zeta = \frac{T_{2s}\Delta s}{h_{o1}-h_{2s}}$.

edge, it produces an over-expansion ahead of the separation point. This expansion will lead to a greater shock strength as discussed later.

Figure 15 shows instantaneous contours of the entropy increase for the studied flows. Here it can be seen that an entropy increase is generated both by the base region and the trailing-edge shocks, with the base region producing the largest part of the entropy increase. The entropy rise within the wake is amplified by the trailing-edge shock, this can be observed as an enlargement of the wake width as it passes the trailing-edge shock.

As discussed before, the over-expansion of the radial-cut trailing edge produces a stronger trailing-edge shock. This can be observed clearly on Fig 15, as the entropy rise produced across the shock is larger as compared to the other two cases.

The mass-averaged loss coefficient has been calculated at specified planes of constant radial coordinates. These values have been then used to determine the loss increase throughout the domain. Loss coefficients have been calculated using the local entropy increase and the mass-weighted enthalpies and isentropic temperature, where local values have been mass-averaged at each plane.

Figure 16 shows two loss coefficient profiles along two selected radial planes. One was chosen to be in the near wake region and the second one on the outlet boundary of the domain (A and B respectively). The profile on the left of the figure shows the mass-averaged loss coefficient in the near wake. Here it can be seen how there is a sharp increase in loss coefficient across the trailing edge shock followed by a large increase in entropy across the wake. The profiles produced by the square-cut and round trailing-edge vanes are similar here, but the profile produced by the radial-cut trailing-edge presents a stronger shock and a shallower wake. On the right figure, the outlet profile can be seen. Here the wake has been diffused by the flow mixing and the interaction with the shock. Again, there is a sharp increase in loss produced by the trailing-edge shock downstream. The overall increased loss observed in the radial-cut trailing-edge case is predominately due to the increase in shock loss.

The mas-averaged loss coefficient values integrated over each plane show that both the round and square-cut trailing-edges produce loss coefficients of $\zeta_A = 0.02$ and $\zeta_B = 0.035$ at the near wake and outlet planes respectively. Comparatively, the radial-cut trailing-edge vane produces loss coefficients a 30% higher ($\zeta_A = 0.021$ and $\zeta_B = 0.044$), and this is due to the over-expansion and subsequent increased shock strength at the trailing-edge. For the other two cases, it appears that the trailing-edge shape does not affect the total loss, and this is consistent with the 1D analysis presented in this paper and in the previous work of Denton and Xu. That is to say that unless the trailing-edge shape is changing significantly the aft suction-surface loading, the trailing-edge shape will not have a significant effect on the total loss produced.

## 7. Conclusions

This paper presented an investigation of dense gas effects and trailing-edge geometry on loss. A 1D analysis of base pressure and mixed-out loss in supersonic wake flow was performed and this found that dense effects tend to increase loss.

Experiments of supersonic wake flows were performed in a Ludwieg tube using a range of gases at similar Mach and Reynolds numbers. The experimental results were used to validate a computational model for such flows. The validation of the CFD models showed that, while RANS simulations could capture changes in the flow produced by different fundamental derivatives, these failed at predicting the base region and near-wake profile. On the other hand, LES modelling showed to highly improve the agreement of the predictions with the experimental data. DES showed an improvement on the flow prediction over RANS, but still underperformed in comparison to LES results.

The results of the experiments and CFD validation showed that both the base regions and base pressure were reduced within the dense gas region. It was demonstrated that a correct modelling of the shear-layer unsteadiness in the base region is important to predicting the trailing-edge flow structure and base pressure.

Finally, a study of the effect shape of trailing-edge shape on vane wake flow and loss was performed using the validated method. This showed that, unless the trailing-edge shape modified the suction-side loading, there appeared to be little effect of trailing-edge shape on loss.

## Acknowledgments

Project supported by the EPSRC (EP/J006394/1, EP/L027437/1) and GE Global Research.

## Nomenclature

| | | | |
|---|---|---|---|
| $A$ | Area | $s$ | Entropy |
| $c$, $c_r$ | Chord, radial chord | $T$, $T_\circ$ | Temperature, total temperature |
| $h$, $h_\circ$ | Enthalpy, total enthalpy | $T_c$ | Critical temperature |
| $M$ | Mach number | $t_{t.e.}$ | Trailing-edge thickness |
| $m$ | Mass flow rate | $t$, $\delta t$ | time, time-step size |
| $p$, $p_\circ$ | Static pressure, total pressure | $V$ | Flow velocity |
| $p_b$ | Base pressure | $\Gamma$ | Fundamental derivative |
| $p_c$ | Critical pressure | $\zeta$ | Loss coefficient |
| $r_{\text{corner}}$ | corner radius | $\theta$ | Angular coordinate |

## References

[1] Anderson W 1991 *AIAA Journal* **29** 2179–2180
[2] Anders J, Anderson W and Murthy A 1999 *Journal of Aircraft* **36** 957–964
[3] Kluwick A 2000 *Philosophical Transactions of the Royal Society of London Series A - Mathematical Physical and Engineering Sciences* **358** 3169–3192
[4] Kluwick A 2004 *Acta mechanica* **169** 123–143
[5] Cinnella P and Congedo P 2007 *Journal of Fluid Mechanics* **580** 179–217
[6] Wheeler A and Ong J 2014 *ASME Turbo Expo* GT2014-25475 (Dusseldrof, Germany)
[7] Durá Galiana F J, Wheeler A and Ong J *ASME Turbo Expo* GT2015-42920 (Montreal, Canada)
[8] Durá Galiana F J, Wheeler A and Ong J 2016 *Journal of Turbomachinery* **138**
[9] Denton J D and Xu L 1990 *Journal of Turbomachinery* **112** 277–285
[10] Lemmon E and Span R 2006 *Journal of Chemical Engineering Data* **51** 785–850